Anisotropic time-domain electronic response in cuprates driven by midinfrared pulses

F. Giusti,[1] A. Montanaro,[1] A. Marciniak,[1] F. Randi,[2] F. Boschini,[3,4] F. Glerean,[1] G. Jarc,[1] H. Eisaki,[5] M. Greven,[6] A. Damascelli,[3] A. Avella,[7] and D. Fausti[1,*]

[1]*Department of Physics, Università degli Studi di Trieste, 34127 Trieste, Italy and Elettra Sincrotrone Trieste S.C.p.A., 34127 Basovizza, Trieste, Italy*

[2]*Joseph Henry Laboratories of Physics, Princeton University, Princeton, New Jersey 08544, USA*

[3]*Quantum Matter Institute, University of British Columbia, Vancouver, BC, Canada V6T 1Z4 and Department of Physics & Astronomy, University of British Columbia, Vancouver, BC, Canada V6T 1Z1*

[4]*Centre Énergie Matériaux Télécommunications, Institut National de la Recherche Scientifique, Varennes, Québec, Canada J3X1S2*

[5]*Nanoelectronics Research Institute, National Institute of Advanced Industrial Science and Technology, Tsukuba, Ibaraki 305-8568, Japan*

[6]*School of Physics and Astronomy, University of Minnesota, Minneapolis, Minnesota 55455, USA*

[7]*Dipartimento di Fisica "E.R. Caianiello," Università degli Studi di Salerno, I-84084 Fisciano (SA), Italy and CNR-SPIN, UOS di Salerno, I-84084 Fisciano (SA), Italy*

(Received 10 December 2020; revised 24 August 2021; accepted 25 August 2021; published 14 September 2021)

Superconductivity in the cuprates is characterized by an anisotropic electronic gap of d-wave symmetry. The aim of this work is to understand how this anisotropy affects the nonequilibrium electronic response of high-T_c superconductors. Here we use a polarization selective time domain experiment to address the dynamics of electronic excitation of different symmetry in optimally doped $Bi_2Sr_2Y_{0.08}Ca_{0.92}Cu_2O_{8+\delta}$ and measure the nodal and antinodal nonequilibrium response resulting from photoexcitations with ultrashort pulses with photon energy comparable to the superconducting gap. The response to long wavelength photoexcitation with pump polarization along the Cu-Cu axis of the sample is discussed with the support of an effective d-wave BCS model which suggests that such transient response could be ascribed to an increase of pair coherence in the antinodal region.

DOI: 10.1103/PhysRevB.104.125121

I. INTRODUCTION

Electronic inhomogeneity [1–10] and an anisotropic superconducting (SC) gap in reciprocal space, which features a d-wave symmetry [11–14], are among the most prominent characteristics of the cuprate superconductors. In d-wave superconductors, the electronic transitions at the antinode are limited to frequencies larger than the SC gap, whereas low-energy excitations are generally allowed at all frequencies at the node, where the SC gap vanishes. This feature dominates the electronic response and differentiates cuprates from conventional s-wave superconductors [15–19]. We recently reported a marked dependence of the response of cuprate superconductors on the polarization of ultrashort light pulses with photon energies comparable to the antinodal SC gap [20]. We revealed that midinfrared pulses at frequencies comparable to the gap energy and polarized along the Cu-Cu direction drive an enhancement of the pump-probe signal commonly associated with the onset of SC.

Here we study the dynamical response of the electronic excitations and of the SC order parameter arising from different regions of the Fermi surface [21]. By selecting the polarizations of the incoming and the outgoing probe beams, we use a Raman-like process to probe excitations with different symmetries and, thereby, demonstrate that the SC gap exhibits a dynamic response that is different in different parts of the first Brillouin zone.

In particular, we study the electronic response of optimally doped $Bi_2Sr_2Y_{0.08}Ca_{0.92}Cu_2O_{8+\delta}$ (Y-Bi2212) across the SC transition following a midinfrared photoexcitation polarized along the Cu-Cu axis and reveal that, whereas antinodal excitations depend strongly on the pump frequency, the nodal ones do not. Our finding indicates that low frequency driven ac currents along the Cu-Cu direction perturb the electronic response associated with antinodal excitations. By comparing this experimental evidence with an effective d-wave symmetry Bardeen-Cooper-Schrieffer (BCS) model, we suggest that long wavelength midinfrared excitations polarized along the Cu-Cu direction may induce a dynamical enhancement of antinodal pair coherence.

II. k-SPACE SELECTION

The electronic Raman scattering measures the total cross section for scattering from all the electrons of the sample illuminated by the incident light. This cross section is determined by the probability that an incident photon with frequency ω_I is scattered into a solid angle interval between θ and $\theta + d\theta$ with a frequency between ω_s and $\omega_s + d\omega_s$. It can be evaluated using time-dependent perturbation theory to the second order [14] and its matrix element related to the transition from the initial I to the final F state can be expressed as

$$M_{FI} = \langle F|R|I\rangle, \tag{1}$$

where R is the Raman tensor and the matrix element $R_{\mu\nu}$ is expressed as a function of the polarization of the incident μ

*daniele.fausti@elettra.eu

TABLE I. Matrix element of the Raman tensor as a function of the incoming and outgoing beam polarization.

α	θ	$R(\alpha,\ \theta)$
0°	0°	$R_{A1g} + R_{B1g}$
45°	45°	$R_{A1g} + R_{B2g}$
90°	90°	$R_{A1g} - R_{B1g}$
0°	90°	R_{B2g}
90°	0°	R_{B2g}
45°	−45°	R_{B1g}
−45°	45°	R_{B1g}

and scattered ν beam. The Raman tensor can be decomposed on the basis of the irreducible representation of the symmetry group of the crystal as

$$R = \sum_n a_n R_{\Gamma_n}, \tag{2}$$

where Γ_n is a representation of the symmetry group [22].

Y-Bi2212 exhibits a bulk superconductivity below $T_c = 97\,\mathrm{K}$, a pseudogap phase between T_c and $T^* = 135\,\mathrm{K}$, and a "strange-metallic" phase above T^* [23]. The SC state is characterized by a maximum SC gap amplitude of $2\Delta(T = 0\,\mathrm{K}) \sim 75\,\mathrm{meV}$ [24]. The Bi-based cuprates are prototypical high-T_c superconductors and their phase diagram has been extensively explored via a variety of equilibrium and time-resolved techniques [22–42].

In the D_{4h} tetragonal point group in the geometry of the experiment, where the beam propagation direction is fixed and perpendicular to the Cu-O plane, the only relevant irreducible representations of the group are A_{1g}, B_{1g}, and B_{2g} and the resulting Raman tensor is [43]

$$R_{\mathrm{Bi2212}} = \frac{1}{2}\begin{bmatrix} R_{A1g} + R_{B1g} & R_{B2g} \\ R_{B2g} & R_{A1g} - R_{B1g} \end{bmatrix}. \tag{3}$$

We introduce the angles α and θ, which represent the polarization directions with respect to the crystallographic Cu-O axis of the input and output beam, respectively. The matrix element of the Raman tensor $R_{\mu\nu} = R(\alpha,\ \theta)$ is calculated on two states, that is, the incoming beam with polarization $\hat{\epsilon}_I \propto \binom{\cos\alpha}{\sin\alpha}$ and the reflected beam $\hat{\epsilon}_F \propto \binom{\cos\theta}{\sin\theta}$. From (3) the Raman matrix element can be expressed by the relation

$$\begin{aligned} R(\alpha,\ \theta) = \tfrac{1}{2}[&R_{A1g}\cos(\alpha - \theta) + R_{B1g}\cos(\alpha + \theta) \\ &+ R_{B2g}\sin(\alpha + \theta)]. \end{aligned} \tag{4}$$

From Eq. (4) one can derive the suitable polarization configurations to select the desired Raman mode. For some significant angles one gets the results in Table I.

The B modes can be selected through crossed polarization configurations ($\theta = \alpha \pm 90°$), whereas the total symmetric mode A_{1g} cannot be singled out by linearly polarized beams, although its relative high intensity renders all other contributions negligible in parallel polarization measurements ($\alpha = \theta$) [43].

Importantly, by changing Raman scattering configurations, one gains sensitivity to different areas of the reciprocal space: While the B_{1g} configuration selects an area close to the d-wave antinode [Fig. 1(c)], the B_{2g} symmetry probes the nodal region [Fig. 1(e)] [14].

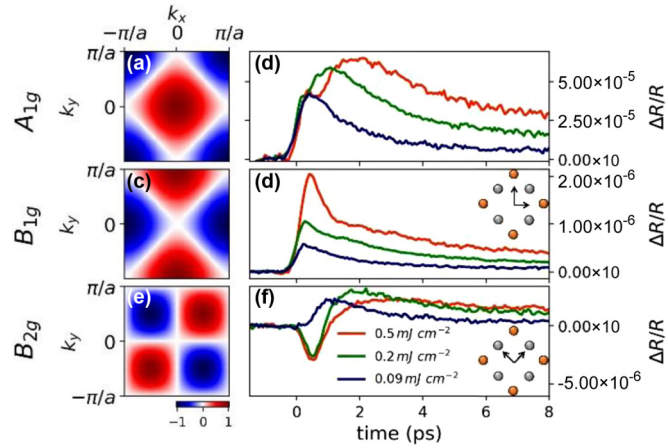

FIG. 1. Polarization selection. Left column: sensitivity to the excitations in the first Brillouin zone for different Raman symmetries [(**a**) A_{1g}, (c) B_{2g}, and (e) B_{1g}]. They represent the weightings $K_i(\mathbf{k})$ of the light-scattering transition for polarization orientations transforming as the three considered symmetries in a D_{4h} crystal [14], and they are defined as (a) $K_{A1g}(\mathbf{k}) = 0.5[\cos(kx) + \cos(kx)]$, (c) $K_{B1g}(\mathbf{k}) = 0.5[\cos(kx) - \cos(kx)]$, and (e) $K_{B2g}(\mathbf{k}) = 0.5[\sin(kx) - \sin(kx)]$. Right column: results of the pump-probe experiment at $T = 80\,\mathrm{K}$ (below T_c) for different excitation fluences. (b) No polarization selection (the dominant contribution is A_{1g}), (d) B_{1g}, and (f) B_{2g}. Three excitation fluences are considered: $0.09\,\mathrm{mJ\,cm^{-2}}$ (blue line) corresponds to the commonly dubbed "linear" response regime, whereas 0.2 and $0.5\,\mathrm{mJ\,cm^{-2}}$ (green and red line, respectively) refer to the "nonlinear" response regime associated with strong perturbation of the SC gap. The inset of panels (d,f) represent sketches of the Cu-O layer of cuprates (the orange dots represent the Cu atoms and the gray ones the oxygen atoms) and the polarization of the incoming and selected probe beams (arrows).

Figure 1 displays the differential reflectivity probed via ultrashort light pulses centered at 1.63 eV with midinfrared excitation polarized along the Cu-Cu axis and different incoming and outgoing polarization selections of the probe: Fig. 1(b) shows polarization integrated measurements (no polarization selection after the interaction with the sample), Fig. 1(d) B_{1g}, and Fig. 1(f) B_{2g} configurations.

These measurements were performed in the SC phase ($T = 80\,\mathrm{K}$) in different excitation intensity regimes. The low-intensity ones (blue lines) are in the "linear" response regime in which the SC order parameter is weakly perturbed. Conversely, higher pump intensities (green and red lines) access the "nonlinear" regime, where the strong perturbation of the SC phase causes a nontrivial composite response. In the latter case, the observed dip in Fig. 1(b) at ≈0.5 ps is usually ascribed to a dynamical melting of the SC phase due to the strength of the photoexcitation [44–48]. Importantly, the time domain response for the different polarization configurations, and consequently for different momentum regions, reveals distinct nonlinear dynamical processes: Whereas the nodal signal [Fig. 1(f)] becomes negative in the first picosecond after the excitation if the pump fluence increases [in correspondence with the dip in Fig. 1(b)], the response around

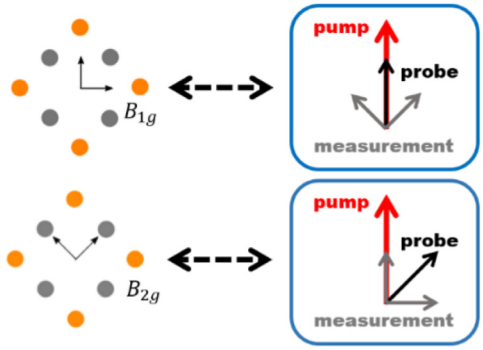

FIG. 2. Measurement correspondence. Correspondence between "standard" pump-probe polarization configurations used to measure B_{1g} and B_{2g} signals (on the left) and birefringence measurements (on the right). The colored dots on the left represent the copper (orange) and oxygen (gray) atoms, whereas the arrows show the polarization of the incoming probe beam and the polarization selection after the sample. In the right panel the polarizations of the birefringence measurement are shown: The black line represents the incoming probe and the gray ones the two final polarization selections after the sample.

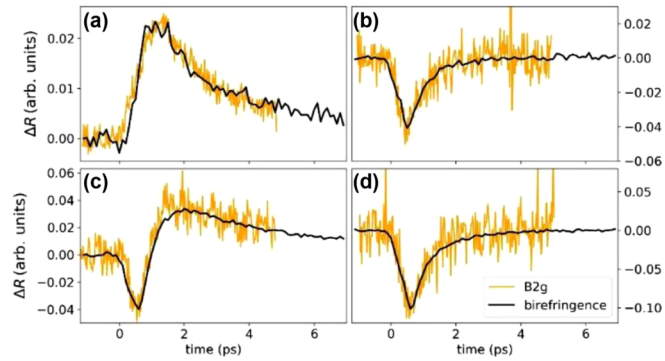

FIG. 3. Measurement comparison. Comparison between a pump-probe measurement performed in B_{2g} configuration (orange line) and a birefringence measurement (black line, obtained by subtracting the polarization components along the Cu-Cu axes), both in superconducting phase (a), (c) and in pseudogap (b),(d). The measurements have been performed in two different pump fluence regimes [0.2 mJ/cm^2 in (a), (b) and 1.3 mJ/cm^2 in (c), (d)]. The signals have been rescaled in order to verify the proportionality between the two measurements.

the antinode [Fig. 1(d)] is sharply enhanced. Therefore, when the photoexcitation is intense enough to perturb the SC state, beyond the linear regime, Fig. 1(b) could be reinterpreted as the result of a composite dynamics, which is affected both by the nodal and antinodal contribution.

III. DETECTION: BIREFRINGENT MEASUREMENTS

The dynamic response changes at 97 K, when the sample exhibits the bulk SC phase. Although the temperature dependence of the pump-probe signal has already been investigated in the cuprates [20,43], few studies of the midinfrared electronic dynamics induced for different areas of the Fermi surface have been performed.

Importantly, continuous temperature scans detecting the weak B_{1g} and B_{2g} pump-probe signals turn out to be very complicated to achieve. This is mostly due to the fact that measurements with incoming and outgoing orthogonal polarizers rely on a homodyning field for the orthogonal emitted field which comes from polarization leakage on the incoming polarizer. This makes the temperature-dependent B_{1g} and B_{2g} pump-probe unfeasible with standard configuration. In the following we propose an alternative method to get their temperature dependence (a similar approach has been exploited in [49]).

Looking at Eq. (4), one notices that the choice of the orthogonal angles α and θ is not the only way to obtain B_{1g} and B_{2g} dynamics. As a matter of fact, the subtraction of two signals with orthogonal θ angles can produce the same result. For example, for $\alpha = 0^\circ$ and $\theta_{1,2} = \pm 45^\circ$ one gets

$$R(\alpha,\ \theta_{1,2}) = \frac{1}{\sqrt{2}}(R_{A1g} + R_{B1g} \pm R_{B2g}), \tag{5}$$

and so $R(\alpha, \theta_1) - R(\alpha, \theta_2) \propto R_{B2g}$ (see Figs. 2 and 3).

Performing the same calculation for $\alpha = 45^\circ$ and $\theta_1 = 0$ and $\theta_2 = 90^\circ$, one gets $R(\alpha, \theta_1) - R(\alpha, \theta_2) \propto R_{B1g}$.

The previous calculations show that birefringent measurements (that is, the detection of the difference between two orthogonal components of the probe pulses reflected or transmitted by the sample) with suitable angles can represent an alternative technique to acquire B_{1g} and B_{2g} signals. In order to check the validity of the alternative method, in Fig. 3 we compare the B_{2g} dynamics measured with the two techniques: The orange line is obtained with the standard configuration ($\alpha = 0^\circ$ and $\theta = 90^\circ$) whereas the black one refers to the birefringence measurement. This configuration is based on intense homodyning fields and therefore is significantly less sensitive to experimental instability. In order to demonstrate the equivalence of the two approaches we show that the two signals are proportional both in the superconducting phase [Figs. 3(a) and 3(c)] and in the pseudogap [Figs. 3(b) and 3(d)] as well as in the two pump fluence regimes [linear: Figs. 3(a) and 3(b); nonlinear: Figs. 3(c) and 3(d)].

Although the crossed polarization measurement and the birefringence one actually provide the same result, the latter is particularly convenient. As a matter of fact, in addition to the weak homodyning field issue discussed, the cross polarization measurements needed to select B_{1g} and B_{2g} signals can also be disturbed by A_{1g} contributions. These are often present because of the high intensity of the A_{1g} signal with respect to the others. On the contrary, in a birefringence measurement the A_{1g} component is split into two contributions, which are equal if the polarization angles $\theta_{1,2}$ are symmetric with respect to the probe polarization α. The final subtraction cancels completely the total symmetric contribution even in the case of small misalignment problems, as the ones produced by continuous temperature measurements.

We performed birefringence time-resolved measurements with suitable input and output polarization directions [$(\alpha,\ \theta_{1,2}) = (0^\circ,\ \pm 45^\circ)$ and $(\alpha,\ \theta_{1,2}) = (45^\circ,\ 0^\circ - 90^\circ)$].

In detail, the orthogonal polarization components of the probe are split by a Wollaston prism after the interaction with the sample. The final signal is the subtraction of the two

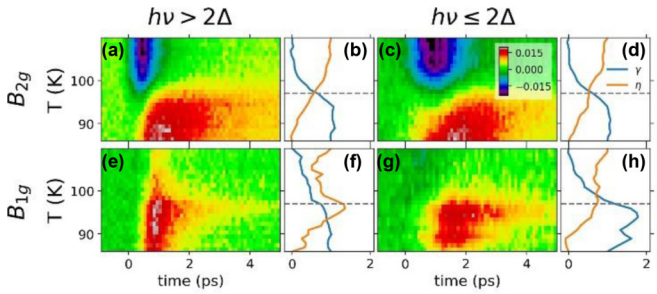

FIG. 4. Temperature dependence for different pump photon energies. Temperature-dependent pump-probe measurements, in B_{2g} and B_{1g} configurations, at low fluence (0.09 mJ cm^{-2}). Top row: B_{2g} measurements with photoexcitation energies of (a) 170 and (c) 70 meV. Panels (b,d) display the values of $\gamma(T)$ and $\eta(T)$ [Eq. (2)] obtained from the data in (a), (c), respectively. The dashed gray lines highlight the critical temperature T_c. Bottom row (e)–(h): same analysis for measurements in the B_{1g} configuration.

projections of the probe beam, performed by a differential photodetector. In the configuration needed to select B_{1g} and B_{2g} symmetries the prism is always oriented such that the measured signal at the equilibrium ($t < 0$) has the same projection on the two axes. All the measurement shown in the following have been performed with birefringent configuration.

IV. EXPERIMENTAL RESULTS

In Fig. 4, we show the results of the measurements for B_{1g} and B_{2g} configurations as a function of temperature. Excitations with energy lower than $2|\Delta|$ (where Δ is the gap amplitude at low temperature) and polarization parallel to the Cu-Cu crystallographic direction result in a peculiar response: Figure 4 shows the response of the system to excitation with photon energies 170 meV ($>2\Delta$) and 70 meV ($<2\Delta$) and fluence $f = 0.09$ mJ cm^{-2}. The variation of the optical properties of the sample is probed by a near-infrared ($h\nu = 1.63$ eV) ultrashort laser pulse.

In Fig. 5 we report the same measurements at higher pump fluence ($f = 0.4$ mJ cm^{-2}).

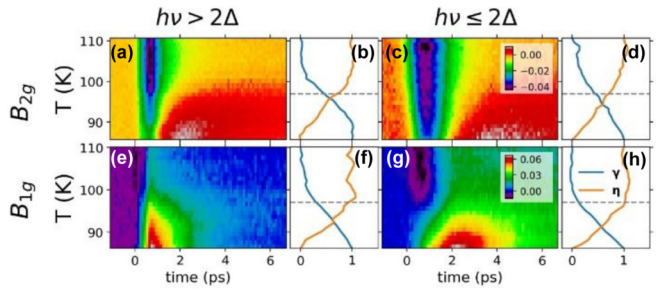

FIG. 5. High-fluence measurements. Temperature-dependent pump-probe measurements, in B_{2g} and B_{1g} configurations, with high fluence excitations (0.4 mJ cm^{-2}). First row: B_{2g} measurements with different excitation photon energies [(a) 170 and (c) 70 meV]. The graphs (b), (d) display the values of $\gamma(T)$ and $\eta(T)$ [Eq. (6)] obtained from the data in (a), (c), respectively. The dashed gray lines represent the critical temperature T_c. The bottom row (e)–(h) shows the same analysis for measurements in the B_{1g} configuration.

V. DATA ANALYSIS

In Fig. 4, we note that both B_{1g} and B_{2g} measurements reveal a different time dependence for the two pump wavelengths which can be partially ascribed to the different time duration of the pump pulses at different wavelength. On the other hand, we note that the B_{1g} signal at different wavelength is qualitatively different while B_{2g} is qualitatively similar for the two-pump wavelength. This is particularly visible above T_c, where the signal produced by pump photon energy $>2\Delta$ is constituted by a residual positive signal at short timescales which is not present for long wavelength excitation. On the contrary, the "nodal" (B_{2g}) signal shows no qualitative difference for the two-pump wavelength [panels (a), (c)].

In order to qualitatively determine the difference between B_{1g} and B_{2g} measurements we propose the following procedure. We fit the signal at a fixed temperature to a linear combination of a SC and a pseudogap time-resolved signal, as described by the relation

$$f(T) = \gamma(T) S_{\mathrm{SC}} + \eta(T) S_{\mathrm{PG}}, \tag{6}$$

where $f(T)$ is the pump-probe signal at temperature T, and $S_{\mathrm{SC}} = f(T = 85\,\mathrm{K})$ and $S_{\mathrm{PG}} = f(T = 110\,\mathrm{K})$ are the signal measured below and above the critical temperature, respectively. In this way, the coefficients $\gamma(T)$ and $\eta(T)$ effectively weight the contributions of the superconducting and pseudogap signals to the response at a given temperature T.

We stress that this procedure does not aim to identify T_c, but it is rather used to obtain a qualitative criterion to compare the response at different wavelength for the two polarization configurations (see Supplemental Material [50]; also see [51]). Importantly, our analysis procedure does not allow for (i) changes in the functional forms of the time-dependent reflectivity (such as the well-known divergence of the decay times at T_c [37]); (ii) the persistence of a pseudogap signal below T_c [35].

On the other hand, it is interesting to note that a divergence in the recovery time of the reflectivity at T_c can be qualitatively described effectively by this approximation. In addition, the qualitative results discussed here do not depend on the arbitrarily chosen temperature (as long as they are well within the two phases). The results of this procedure are displayed in Figs. 4(b), 4(d), 4(f), and 4(h).

In spite of the qualitative nature of this analysis, we argue that the temperature dependence of $\gamma(T)$ and $\eta(T)$ captures the main transition between the signals coming from SC and the pseudogap phases. The curves of the two parameters cross at the critical temperature $T_c = 97$ K for nodal measurements at low fluence [Figs. 2(b) and 2(d)]. The same behaviors occur when no polarization selection is applied to the probe after the interaction with the sample (see Supplemental Material [50]).

Figures 4(b) and 4(d) confirm that the overall transient response in the nodal region of the Brillouin zone is not affected by the pump photon energy. On the contrary, in the antinodal region [Figures 4(f) and (h)], the crossing temperature between the fit parameters strongly depends on the photon energy. In particular, for high pump photon energy the pseudogap contribution dominates, whereas for low photon energies the SC contribution prevails for a few K above T_c. This suggests that the region in momentum space relevant to

the observed onset of a superconductivelike signal about T_c is the antinodal region.

The analysis performed on higher pump fluence measurements provides a consistent outcome. In particular, the results reported in Figs. 5(b), 5(d), 5(f), and 5(h) suggest that the crossing between the two parameters, which for lower pump fluence occurs at the transition temperature, at least in the nodal case, is shifted to lower temperatures. We interpret this behavior as the effect of the strong nonlinear excitation produced by the pump pulse, which is able to dynamically perturb (and destroy) the superconducting phase, resulting in an effective decrease of the measured T_c. Interestingly, the effect is much more visible when we select the response of the antinodal region [B_{1g} configuration, Figs. 5(f) and 5(h)], where the SC gap has its maximum value at the equilibrium, with respect to the nodal one [B_{2g} symmetry, Figs. 5(b) and 5(d)]. We stress that the analysis in terms of the linear combination of superconducting and pseudogap signal should not be considered as a precise identification of the SC transition temperature but rather seen as a means to visually compare the different temperature maps.

VI. DISCUSSION: EFFECTIVE BCS MODEL

In order to interpret these results, we propose an effective d-wave BCS model, which qualitatively describes the dynamics of the sample after the interaction with a low-energy pump pulse ($h\nu \sim 2\Delta$). It is well known that the BCS formalism cannot describe the whole cuprate phenomenology, since it does not take into account electronic correlations nor dissipations. The aim of this calculation is to describe the coherent interaction between the pulsed electric field and the d-wave superconductor and to draw a picture of the possible scenario emerging from the anisotropic response of the condensate in the first few hundreds of femtoseconds after a low photon energy excitation. In this short timescale both dissipation effects (such as phonon scattering) and Coulomb $e-e$ interaction are neglected.

The Hamiltonian can be written as

$$H = \sum_k \varepsilon\left[\mathbf{k} - \frac{e}{\hbar}A(t)\boldsymbol{\chi}\right]\hat{n}(\mathbf{k}) + \sum_k \Delta^*(\mathbf{k})\psi_{\mathbf{k}} + \Delta(\mathbf{k})\psi^\dagger_{\mathbf{k}}, \tag{7}$$

where $\varepsilon(\mathbf{k}) = -2t(\cos k_x + \cos k_y)$ is the two-dimensional tight binding electronic dispersion, $A(t)$ is the vector potential of the pump pulse, and χ is its polarization. Finally $\Delta(\mathbf{k}) = \zeta(\mathbf{k})|\Delta|e^{i\theta}$ [where $\zeta(\mathbf{k}) = \frac{1}{2}(\cos k_x + \cos k_y)$ parametrizes the d-wave momentum dependence of the gap function; $|\Delta|$ is the amplitude of the gap and θ its phase] is the gap function, whose dependence on k remarks its d-wave anisotropy, and $\psi(\mathbf{k}) = \hat{c}_\uparrow(\mathbf{k})\hat{c}_\downarrow(-\mathbf{k})$ is the pair operator.

All calculations of the dynamical response have been performed within the density matrix theory framework, which gives the following set of relevant equations,

$$\begin{aligned} i\hbar\frac{\partial}{\partial t}\bar{n}(\mathbf{k}) &= \Delta(\mathbf{k})\Lambda^*(\mathbf{k}) - \Delta^*(\mathbf{k})\Lambda(\mathbf{k}) \\ i\hbar\frac{\partial}{\partial t}\Lambda(\mathbf{k}) &= \left\{\varepsilon\left[\mathbf{k} - \frac{e}{\hbar}A(t)\boldsymbol{\chi}\right] + \varepsilon\left[\mathbf{k} - \frac{e}{\hbar}A(t)\boldsymbol{\chi}\right]\right\} \\ &\quad \times\Lambda(\mathbf{k}) + \Delta(\mathbf{k})[1 - 2\bar{n}(\mathbf{k})], \end{aligned} \tag{8}$$

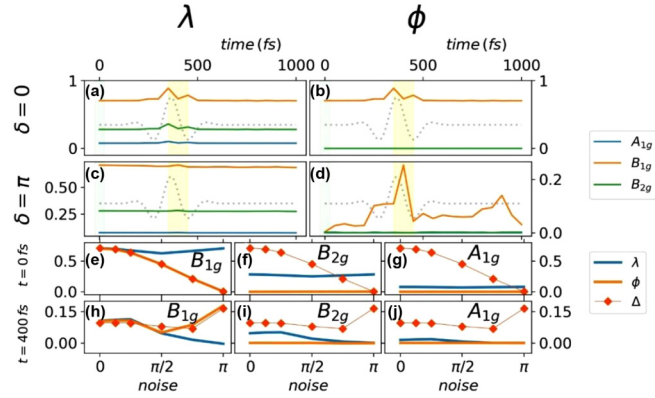

FIG. 6. Theoretical effective model. In (a), (b), the dynamics of $\lambda_i = \int_{\mathrm{BZ}} |\Lambda(\mathbf{k})| \cdot |\mathrm{K_i}(\mathbf{k})| d\mathbf{k}$ and $\phi_i = |\int_{\mathrm{BZ}} \Lambda(\mathbf{k}) \cdot \mathrm{K_i}(\mathbf{k}) d\mathbf{k}|$ are displayed, where $i = A_{1g}$, B_{1g}, B_{2g} and $K_i(\mathbf{k})$ represent the weightings of the light-scattering transition defined in Fig. 1. The blue line represents the A_{1g} selection, the orange line the B_{1g} one, and the green curve the B_{2g} one. The dashed line shows the time evolution of the pump pulse. In (c), (d), random noise with amplitude $\delta = \pi$ was added to the pair operator phase, in order to simulate an initial pseudogap state. In (e)–(j) the noise dependence of three quantities λ in blue, ϕ in orange, and the superconducting gap with the red diamonds) is analyzed for two time delays: at the equilibrium (e)–(g) and immediately after the pump excitation (h)–(j).

where $\bar{n}(\mathbf{k}) = \langle n_\uparrow(\mathbf{k})\rangle = \langle n_\downarrow(\mathbf{k})\rangle$ and $n_\sigma(\mathbf{k})$ is the number operator for the spin σ of the Wannier electronic state with momentum $\mathbf{k}$, and $\Lambda(\mathbf{k}) = \langle\psi_k\rangle$ is the pair operator expectation value [see [20] for further details].

To compare the model with the experimental data, we computed the dynamics of the pair operator expectation value $\Lambda(\mathbf{k})$ and tracked the abundance and the coherence of the pairs.

We are interested in these two observables, since they may be linked to the signatures of superconducting fluctuations at temperatures larger than T_c, typical of cuprates [47]. This anomalous behavior is sometimes interpreted as the persistence of Cooper pairs losing phase coherence: In this picture the transition to the pseudogap phase is associated with the vanishing of the macroscopic coherence above the transition temperature and not to the weakening of pair strength [52–59].

In particular, we extracted two quantities: λ, the integral over the first Brillouin zone of the pair operator absolute value, which measures the abundance of pairs without considering their mutual and overall d-wave phase coherence; and ϕ, the absolute value of its integral, which measures the abundance of d-wave coherent pairs. Importantly, the contribution to the electronic response coming from excitation of different symmetry-select specific regions (and signs for ϕ) in the Brillouin zone, we computed these quantities by integrating with (the absolute value in the λ case) A_{1g}, B_{1g}, or B_{2g} kernels [see Figs. 1(a), 1(c), and 1(e)] and simulate the results of the related symmetry-selective experiments.

The curves in Fig. 6(a) show at time $t = 0$ an initial number of pairs that depend on the symmetry selection as well as a time-dependent increase of their number that is correlated with the pump excitation ($t = 350$ fs). The calculations reveal an enhancement of the number of pairs much stronger in the

antinodal region in agreement with the experiment. A similar dynamical response is shown by the different contributions to the SC gap in Fig. 6(b), which unveil the prevalent effect of the preservation of the phase coherence over the increase of the number of pairs.

In order to describe the dynamical response above T_c, we propose to modify the equilibrium state of the BCS superconductor by introducing "artificial" phase incoherence, which could effectively mimic the presence of inhomogeneities in the system. This choice is justified by the evidence that in this temperature range SC fluctuations may persist, while macroscopic superconducting coherence is lost [52–59]. In the calculations, we add a uniform random noise to the phase of the expectation value of the pair operator [20].

The dependence of the amplitude of the SC gap on the noise amplitude δ is shown in Fig. 6(e) (red diamonds), where the noise increase determines the complete collapse of the superconducting gap (for $\delta = \pi$), despite the presence of pairs. Figures 6(e)–6(g) show also that at the equilibrium the dominant contribution to the gap amplitude comes from the antinodal region [orange line in Fig. 6(e)] for any coherence condition.

By considering this initial arbitrary state with maximum incoherence ($\delta = \pi$) and letting it evolve through our modified BCS Hamiltonian, we obtain the dynamical response for the different symmetries shown in Figs. 6(c) and 6(d). In this scenario, the pairs' abundance is much less affected by the pump excitation for any geometry [Fig. 6(c)]. On the contrary, a different behavior is observed for the SC gap: In the B_{2g} and A_{1g} configurations we observe a negligible modification of the gap induced by the pump, whereas the B_{1g} contribution from the initial zero value ($t = 0$ fs) increases sharply around $t = 300$ fs [Fig. 6(c)]. These results suggest that a low photon energy excitation may be able to dynamically restore phase coherence in the antinodal region of the system.

VII. CONCLUSION

In conclusion, we studied the dynamical response of electronic excitations in optimally doped Y-Bi2212. By properly combining the polarization of the incoming and scattered probe beam, we were able to isolate the contributions to the pump wavelength dependence of the SC response observed in [20], coming from different regions of the Fermi surface. In contrast to the nodal signal, the response at the antinodes is strongly dependent on the pump photon energy. Our effective model suggests that low photon energy excitation polarization and driving currents along the Cu-Cu direction affect the Cooper pair density only slightly (and do not above T_c), but they may dynamically induce pair coherence in the antinodal region of the Fermi surface (both above and below T_c). In the presence of an inhomogeneous system above T_c, this could give rise to a nonzero superconducting gap and superconductinglike behaviors, which might contribute to the observed light-driven coherent transport above T_c [60–69]. Finally, we stress that the possibility to enhance d-wave phase coherence at the antinodes through driven currents in the Cu-Cu direction may be of relevance for understanding both equilibrium and nonequilibrium properties of unconventional superconductors.

ACKNOWLEDGMENTS

This work was mainly supported by the European Commission through the ERCStG2015, INCEPT, Grant No. 677488. A.A. acknowledges support by MIUR under Project No. PRIN 2017RKWTMY. This research was undertaken thanks in part to funding from the Max Planck UBC Centre for Quantum Materials and the Canada First Research Excellence Fund, Quantum Materials and Future Technologies Program. The work at UBC was supported by the Killam, Alfred P. Sloan, and Natural Sciences and Engineering Research Council of Canada (NSERC) Steacie Memorial Fellowships (A.D.), the Alexander von Humboldt Fellowship (A.D.), the Canada Research Chairs Program (A.D.), NSERC, Canada Foundation for Innovation (CFI), and CIFAR Quantum Materials Program. The work at the University of Minnesota was funded by the Department of Energy through the University of Minnesota Center for Quantum Materials under Grant No. DE-SC-0016371. D.F. acknowledges support by MIUR under Project No. PRIN 2017BZPKSZ.

[1] J. W. Alldredge, K. Fujita, H. Eisaki, S. Uchida, and K. McElroy, Universal disorder in $Bi_2Sr_2CaCu_2O_{8+x}$, Phys. Rev. B **87**, 104520 (2013).

[2] D. Pelc, Z. Anderson, B. Yu, C. Leighton, and M. Greven, Universal superconducting precursor in three classes of unconventional superconductors, Nat. Commun. **10**, 2729 (2019).

[3] D. Pelc, M. Vučković, M. S. Grbić, M. Požek, G. Yu, T. Sasagawa, M. Greven, and Neven Barišić, Emergence of superconductivity in the cuprates via a universal percolation process, Nat. Commun. **9**, 4327 (2018).

[4] P. Popčević, D. Pelc, Y. Tang, K. Velebit, Z. Anderson, V. Nagarajan, G. Yu, M. Požek, N. Barišić, and M. Greven, Percolative nature of the direct-current paraconductivity in cuprate superconductors, Quantum Mater. **3**, 42 (2018).

[5] D. Pelc, P. Popčević, M. Požek,M. Greven, and N. Barišić, Unusual behavior of cuprates explained by heterogeneous charge localization, Sci. Adv. **5**, eaau4538 (2019).

[6] P. M. Singer, A. W. Hunt, and T. Imai, $^{6}3$Cu NQR Evidence for Spatial Variation of Hole Concentration in $La_{2-x}Sr_xCuO_4$, Phys. Rev. Lett. **88**, 047602 (2002).

[7] J. Bobroff, H. Alloul, S. Ouazi, P. Mendels, A. Mahajan, N. Blanchard, G. Collin, V. Guillen, and J.-F. Marucco, Absence of Static Phase Separation in the High T_c Cuprate $YBa_2Cu_3O_{6+y}$, Phys. Rev. Lett. **89**, 157002 (2002).

[8] J. C. Phillips, A. Saxena, and A. R. Bishop, Pseudogaps, dopants, and strong disorder in cuprate high-temperature superconductors, Rep. Prog. Phys. **66**, 2111 (2003).

[9] Ø. Fischer, M. Kugler, I. Maggio-Aprile, C. Berthod, and C. Renner, Scanning tunneling spectroscopy of high-temperature superconductors, Rev. Mod. Phys. **79**, 353 (2007).

[10] G. Yu, D.-D. Xia, D. Pelc, R.-H. He, N.-H. Kaneko, T. Sasagawa, Y. Li, X. Zhao, N. Barišić, A. Shekhter, and M. Greven, Universal precursor of superconductivity in the cuprates, Phys. Rev. B **99**, 214502 (2019).

[11] D. J. Scalapino, E. Loh, Jr., and J. E. Hirsch, d-wave pairing near a spin-density-wave instability, Phys. Rev. B **34**, 8190(R) (1986).

[12] P. Monthoux, A. V. Balatsky, and D. Pines, Toward a Theory of High-Temperature Superconductivity in the Antiferromagnetically Correlated Cuprate Oxides, Phys. Rev. Lett. **67**, 3448 (1991).

[13] T. P. Devereaux, D. Einzel, B. Stadlober, R. Hackl, D. H. Leach, and J. J. Neumeier, Electronic Raman Scattering in High-T_c Superconductors: A Probe of $d_x^2-y^2$ Pairing, Phys. Rev. Lett. **72**, 396 (1994).

[14] T. P. Devereaux and D. Einzel, Electronic Raman scattering in superconductors as a probe of anisotropic electron pairing, Phys. Rev. B **51**, 16336 (1995); **54**, 15547(E) (1996).

[15] F. Cilento *et al.*, Photo-enhanced antinodal conductivity in the pseudogap state of high-T_c cuprates, Nat. Commun. **5**, 4353 (2014).

[16] E. J. Nicol and J. P. Carbotte, Comparison of s- and d-wave gap symmetry in nonequilibrium superconductivity, Phys. Rev. B **67**, 214506 (2003).

[17] V. V. Kabanov, J. Demsar, B. Podobnik, and D. Mihailovic, Quasiparticle relaxation dynamics in superconductors with different gap structures: Theory and experiments on $YBa_2Cu_3O_{7-\delta}$, Phys. Rev. B **59**, 1497 (1999).

[18] R. Cortés, L. Rettig, Y. Yoshida, H. Eisaki, M. Wolf, and U. Bovensiepen, Momentum-Resolved Ultrafast Electron Dynamics in Superconducting $Bi_2Sr_2CaCu_2O_{8+\delta}$, Phys. Rev. Lett. **107**, 097002 (2011).

[19] C. L. Smallwood, J. P. Hinton, C. J. Wentao Zhang, J. D. Koralek, H. Eisaki, D.-H. Lee, J. Orenstein, and A. Lanzara, Tracking Cooper pairs in a cuprate superconductor by ultrafast angle-resolved photoemission, Science **336**, 1137 (2012).

[20] F. Giusti, A. Marciniak, F. Randi, G. Sparapassi, F. Boschini, H. Eisaki, M. Greven, A. Damascelli, A. Avella, and D. Fausti, Signatures of Enhanced Superconducting Phase Coherence in Optimally Doped $Bi_2Sr_2Y_{0.08}Ca_{0.92}Cu_2O_{8+\delta}$ Driven by Midinfrared Pulse Excitations, Phys. Rev. Lett. **122**, 067002 (2019).

[21] T. P. Devereaux and R. Hackl, Inelastic light scattering from correlated electrons, Rev. Mod. Phys. **79**, 175 (2007).

[22] J. Yang, Ph.D. thesis, University of Colorado, Boulder, 2017.

[23] F. Cilento, S. Dal Conte, G. Coslovich, F. Banfi, G. Ferrini, H. Eisaki, M. Greven, A. Damascelli, D. van der Marel, F. Parmigiani, and C. Giannetti, In search for the pairing glue in cuprates by non-equilibrium optical spectroscopy, J. Phys.: Conf. Ser. **449**, 012003 (2013).

[24] W. S. Lee, I. M. Vishik, K. Tanaka, D. H. Lu, T. Sasagawa, N. Nagaosa, T. P. Devereaux, Z. Hussain, and Z.-X. Shen, Abrupt onset of a second energy gap at the superconducting transition of underdoped Bi2212, Nature (London, UK) **450**, 81 (2007).

[25] D. N. Basov and T. Timusk, Electrodynamics of high-T_c superconductors, Rev. Mod. Phys. **77**, 721 (2005).

[26] H. J. A. Molegraaf, C. Presura, D. van der Marel, P. H. Kes, and M. Li, Superconductivity-induced transfer of in-plane spectral weight in $Bi_2Sr_2CaCu_2O_{8+\delta}$, Science **295**, 2239 (2002).

[27] C. Giannetti *et al.*, Revealing the high-energy electronic excitations underlying the onset of high-temperature superconductivity in cuprates, Nat. Commun. **2**, 353 (2011).

[28] L. Li, Y. Wang, S. Komiya, S. Ono, Y. Ando, G. D. Gu, and N. P. Ong, Diamagnetism and Cooper pairing above T_c in cuprates, Phys. Rev B **81**, 054510 (2010).

[29] R. A. Kaindl, M. A. Carnahan, D. S. Chemla, S. Oh, and J. N. Eckstein, Dynamics of Cooper pair formation in $Bi_2Sr_2CaCu_2O_{8+\delta}$, Phys. Rev B **72**, 060510(R) (2005).

[30] M. P. A. Fisher and D. H. Lee, Correspondence between two-dimensional bosons and a bulk superconductor in a magnetic field, Phys. Rev B **39**, 2756 (1989).

[31] Y. Hwu, L. Lozzi, M. Marsi, S. La Rosa, M. Winokur, P. Davis, M. Onellion, H. Berger, F. Gozzo, F. Lévy, and G. Margaritondo, Electronic Spectrum of the High-Temperature Superconducting State, Phys. Rev. Lett. **67**, 2573 (1991).

[32] H. Anzai, A. Ino, M. Arita, H. Namatame, M. Taniguchi, M. Ishikado, K. Fujita, S. Ishida, and S. Uchida, Relation between the nodal and antinodal gap and critical temperature in superconducting Bi2212, Nat. Commun. **4**, 1815 (2013).

[33] E. Schachinger and J. P. Carbotte, Coupling to spin fluctuations from conductivity scattering rates, Phys. Rev B **62**, 9054 (2000).

[34] W. Zhang, C. L. Smallwood, C. Jozwiak, T. L. Miller, Y. Yoshida, H. Eisaki, D.-H. Lee, and A. Lanzara, Signatures of superconductivity and pseudogap formation in nonequilibrium nodal quasiparticles revealed by ultrafast angle-resolved photoemission, Phys. Rev B **88**, 245132 (2013).

[35] G. Coslovich, C. Giannetti, F. Cilento, S. Dal Conte, T. Abebaw, D. Bossini, G. Ferrini, H. Eisaki, M. Greven, A. Damascelli, and F. Parmigiani, Competition between the Pseudogap and Superconducting States of $Bi_2Sr_2Ca_{0.92}Y_{0.08}Cu_2O_{8+\delta}$ Single Crystals Revealed by Ultrafast Broadband Optical Reflectivity, Phys. Rev. Lett. **110**, 107003 (2013).

[36] F. Liu and G. F. Mazenko, Growth kinetics of systems with continuous symmetry, Phys. Rev. B **45**, 6989 (1992).

[37] C. Giannetti, M. Capone, D. Fausti, M. Fabrizio, F. Parmigiani, and D. Mihailovic, Ultrafast optical spectroscopy of strongly correlated materials and high-temperature superconductors: A non-equilibrium approach, Adv. Phys. **65**, 58 (2016).

[38] C. Thomsen and G. Kaczmarczyk, in *Handbook of Vibrational Spectroscopy*, edited by J. M. Chalmers and P. R. Griffiths (John Wiley & Sons, Chichester, UK, 2002).

[39] J. D. Rameau *et al.*, Energy dissipation from a correlated system driven out of equilibrium, Nat. Commun. **7**, 13761 (2016).

[40] T. Konstantinova *et al.*, Nonequilibrium electron and lattice dynamics of strongly correlated $Bi_2Sr_2CaCu_2O_{8+\delta}$ single crystals, Sci. Adv. **4**, eaap7427 (2018).

[41] H. Eisaki, N. Kaneko, D. L. Feng, A. Damascelli, P. K. Mang, K. M. Shen, Z.-X. Shen, and M. Greven, Effect of chemical inhomogeneity in bismuth-based copper oxide superconductors, Phys. Rev. B **69**, 064512 (2004).

[42] B. Mansart, J. Lorenzana, A. Mann, A. Odeh, M. Scarongella, M. Chergui, and F. Carbone, Coupling of a high-energy excitation to superconducting quasiparticles in a cuprate from coherent charge fluctuation spectroscopy, Proc. Natl. Acad. Sci. USA **110**, 4539 (2013).

[43] Y. Toda, F. Kawanokami, T. Kurosawa, M. Oda, I. Madan, T. Mertelj, V. V. Kabanov, and D. Mihailovic, Rotational symmetry breaking in $Bi_2Sr_2CaCu_2O_{8+\delta}$ probed by polarized femtosecond spectroscopy, Phys. Rev. B **90**, 094513 (2014).

[44] I. Madan, T. Kurosawa, Y. Toda, M. Oda, T. Mertelj, P. Kusar, and D. Mihailovic, Separating pairing from quantum phase coherence dynamics above the superconducting transition by femtosecond spectroscopy, Sci. Rep. **4**, 5656 (2014).

[45] P. Kusar, V. V. Kabanov, J. Demsar, T. Mertelj, S. Sugai, and D. Mihailovic, Controlled Vaporization of the Superconducting Condensate in Cuprate Superconductors by Femtosecond Photoexcitation, Phys. Rev. Lett. **101**, 227001 (2008).

[46] L. R. Testardi, Destruction of superconductivity by laser light, Phys. Rev. B **4**, 2189 (1971).

[47] C. Giannetti, G. Coslovich, F. Cilento, G. Ferrini, H. Eisaki, N. Kaneko, M. Greven, and F. Parmigiani, Discontinuity of the ultrafast electronic response of underdoped superconducting $Bi_2Sr_2CaCu_2O_{8+\delta}$ strongly excited by ultrashort light pulses, Phys. Rev. B **79**, 224502 (2009).

[48] L. Stojchevska, P. Kusar, T. Mertelj, V. V. Kabanov, Y. Toda, X. Yao, and D. Mihailovic, Mechanisms of nonthermal destruction of the superconducting state and melting of the charge-density-wave state by femtosecond laser pulses, Phys. Rev. B **84**, 180507(R) (2011).

[49] I. Madan, V. V. Baranov, Y. Toda, M. Oda, T. Kurosawa, V. V. Kabanov, T. Mertelj, and D. Mihailovic, Dynamics of superconducting order parameter through ultrafast normal-to-superconducting phase transition in $Bi_2Sr_2CaCu_2O_{8+\delta}$ from multipulse polarization-resolved transient optical reflectivity, Phys. Rev. B **96**, 184522 (2017).

[50] See Supplemental Material at http://link.aps.org/supplemental/10.1103/PhysRevB.104.125121 for details on the fitting procedure; also see Ref. [51].

[51] M. A. Quijada, D. B. Tanner, R. J. Kelley, M. Onellion, H. Berger, and G. Margaritondo, Anisotropy in the *ab*-plane optical properties of $Bi_2Sr_2CaCu_2O_8$ single-domain crystals, Phys. Rev. B **60**, 14917 (1999).

[52] L. Perfetti, B. Sciolla, G. Biroli, C. J. van der Beek, C. Piovera, M. Wolf, and T. Kampfrath, Ultrafast Dynamics of Fluctuations in High-Temperature Superconductors Far from Equilibrium, Phys. Rev. Lett. **114**, 067003 (2015).

[53] J. Corson, R. Mallozzi, J. Orenstein, J. N. Eckstein, and I. Bozovic, Vanishing of phase coherence in underdoped $Bi_2Sr_2CaCu_2O_{8+\delta}$, Nature (London, UK) **398**, 221 (1999).

[54] F. Boschini *et al.*, Collapse of superconductivity in cuprates via ultrafast quenching of phase coherence, Nat. Mater. **17**, 416 (2018).

[55] T. Kondo *et al.*, Point nodes persisting far beyond T_c in Bi2212, Nat. Commun. **6**, 7699 (2015).

[56] M. S. Grbić, N. Barišić, A. Dulčić, I. Kupčić, Y. Li, X. Zhao, G. Yu, M. Dressel, M. Greven, and M. Požek, Microwave measurements of the in-plane and *c*-axis conductivity in $HgBa_2CuO_{4+\delta}$: Discriminating between superconducting fluctuations and pseudogap effects, Phys. Rev. B **80**, 094511 (2009).

[57] L. Bilbro, R. Aguilar, G. Logvenov, O. Pelleg, I. Božović, and N. P. Armitage, Temporal correlations of superconductivity above the transition temperature in $La_{2-x}Sr_xCuO_4$ probed by terahertz spectroscopy, Nat. Phys. **7**, 298 (2011).

[58] J. Orenstein, J. Corson, S. Oh, and J. N. Eckstein, Superconducting fluctuations in $Bi_2Sr_2Ca_{1-x}Dy_xCu_2O_{8+\delta}$ as seen by terahertz spectroscopy, Ann. Phys. **15**, 596 (2006).

[59] I. Kokanović, D. J. Hills, M. L. Sutherland, R. Liang, and J. R. Cooper, Diamagnetism of $YBa_2Cu_3O_{6+x}$ crystals above T_c: Evidence for Gaussian fluctuations, Phys. Rev. B **88**, 060505(R) (2013).

[60] D. Fausti, R. I. Tobey, N. Dean, S. Kaiser, A. Dienst, M. C. Hoffmann, S. Pyon, T. Takayama, H. Takagi, and A. Cavalleri, Light-induced superconductivity in a stripe-ordered cuprate, Science **331**, 189 (2011).

[61] S. Kaiser, C. R. Hunt, D. Nicoletti, W. Hu, I. Gierz, H. Y. Liu, M. Le Tacon, T. Loew, D. Haug, B. Keimer, and A. Cavalleri, Optically induced coherent transport far above T_c in underdoped $YBa_2Cu_3O_{6+\delta}$, Phys. Rev. B **89**, 184516 (2014).

[62] W. Hu, S. Kaiser, D. Nicoletti, C. R. Hunt, I. Gierz, M. C. Hoffmann, M. Le Tacon, T. Loew, B. Keimer, and A. Cavalleri, Optically enhanced coherent transport in $YBa_2Cu_3O_{6.5}$ by ultrafast redistribution of interlayer coupling, Nat. Mater. **13**, 705 (2014).

[63] E. Casandruc, D. Nicoletti, S. Rajasekaran, Y. Laplace, V. Khanna, G. D. Gu, J. P. Hill, and A. Cavalleri, Wavelength-dependent optical enhancement of superconducting interlayer coupling in $La_{1.885}Ba_{0.115}CuO_4$, Phys. Rev. B **91**, 174502 (2015).

[64] M. Mitrano, A. Cantaluppi, D. Nicoletti, S. Kaiser, A. Perucchi, S. Lupi, P. Di Pietro, D. Pontiroli, M. Riccò, S. R. Clark, D. Jaksch, and A. Cavalleri, Possible light-induced superconductivity in K_3C_{60} at high temperature, Nature **530**, 461 (2016).

[65] M. Budden *et al.*, Evidence for metastable photo-induced superconductivity in K_3C_{60}, arXiv:2002.12835.

[66] B. Liu, M. Först, M. Fechner, D. Nicoletti, J. Porras, T. Loew, B. Keimer, and A. Cavalleri, Pump Frequency Resonances for Light-Induced Incipient Superconductivity in $YBa_2Cu_3O_{6.5}$, Phys. Rev X **10**, 011053 (2020).

[67] M. Buzzi, D. Nicoletti, M. Fechner, N. Tancogne-Dejean, M. A. Sentef, A. Georges, T. Biesner, E. Uykur, M. Dressel, A. Henderson *et al.*, Photomolecular High-Temperature Superconductivity, Phys. Rev. X **10**, 031028 (2020).

[68] J. Tindall, F. Schlawin, M. Buzzi, D. Nicoletti, J. R. Coulthard, H. Gao, A. Cavalleri, M. A. Sentef, and D. Jaksch, Dynamical order and superconductivity in a frustrated many-body system, Phys. Rev. Lett. **125**, 137001 (2020).

[69] F. Novelli, G. Giovannetti, A. Avella, F. Cilento, L. Patthey, M. Radovic, M. Capone, F. Parmigiani, and D. Fausti, Localized vibrations in superconducting $YBa_2Cu_3O_7$ revealed by ultrafast optical coherent spectroscopy, Phys. Rev. B **95**, 174524 (2017).